Design and Implementation of Low-Profile Contactless Battery Charger Using Planar Printed Circuit Board Windings as Energy Transfer Device

5 authors, including:

Honnyong Cha
Kyungpook National University
101 PUBLICATIONS **1,229** CITATIONS

Design and Implementation of Low-Profile Contactless Battery Charger Using Planar Printed Circuit Board Windings as Energy Transfer Device

Byungcho Choi, *Member, IEEE*, Jaehyun Nho, Honnyong Cha, Taeyoung Ahn, *Member, IEEE*, and Seungwon Choi, *Member, IEEE*

Abstract—This paper paper presents the practical details involved in the design and implementation of a contactless battery charger that employs a pair of neighboring printed circuit board (PCB) windings as a contactless energy transfer device. A prototype contactless battery charger developed for application with cellular phones is used as an example to address the design considerations for the PCB windings and energy transfer circuit, plus demonstrates the performance of the contactless charger adapted to a practical application system.

Index Terms—Contactless battery charger for cellular phones, contactless energy transfer, coupled printed circuit board (PCB) windings.

I. INTRODUCTION

EARLIER studies [1]–[3] have shown that substantial inductive coupling exists between two spiral windings printed on the opposite sides of a double-sided printed circuit board (PCB). Accordingly, a doubled-sided PCB with spiral windings on its surfaces can be used as a substitute for a conventional core-based transformer in certain low-to-medium power applications, for example, isolated gate drive circuits for MOSFETs/insulated gate bipolar transistors (IGBTs) [2] and low-profile dc-to-dc converters [3]. More recently, an attempt [4], [5] was made to utilize the inductive coupling between two neighboring PCB windings as a means of a contactless energy transfer. In the aforementioned study, two separate PCB windings (each built on a single-sided PCB) are placed closely in parallel, as shown in Fig. 1(a), to make them function as an
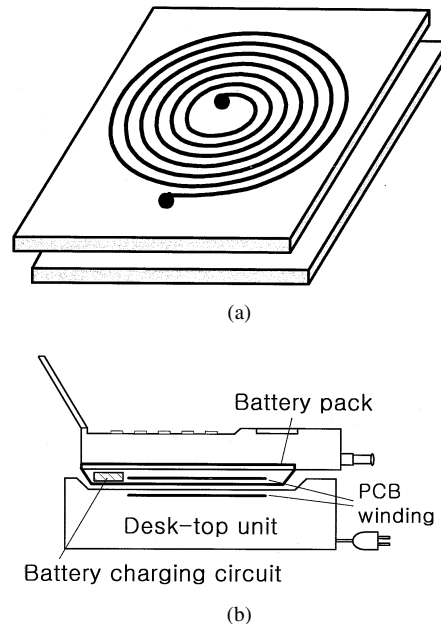
Fig. 1. Neighboring PCB windings and contactless charger for cellular phones. (a) Neighboring PCB windings. (b) Contactless charger developed for cellular phones.

energy transfer device. The feasibility of a contactless energy transfer using PCB windings was reported in [4], and the idea of adapting this contactless energy transfer scheme to battery charging circuits for portable electronics was presented in [5] along with preliminary results on such an application. Fig. 1(b) shows the configuration of the contactless battery charger proposed in [5] for application to cellular phones. The desk-top unit, i.e., the primary side of the charger, contains the primary PCB winding along with associated electronics, while the secondary side of the charger consists of the secondary PCB winding, a battery charging circuit, and lithium-ion battery. The inductive coupling between these two paralleled PCB windings, one on top of the desk-top unit and the other on the bottom of the battery pack, provides a contactless energy transfer. One apparent merit of the proposed charging method is that the charger does not noticeably increase the thickness, size, or weight of the application system, thereby making it adaptable to low-profile hand-held electronics.
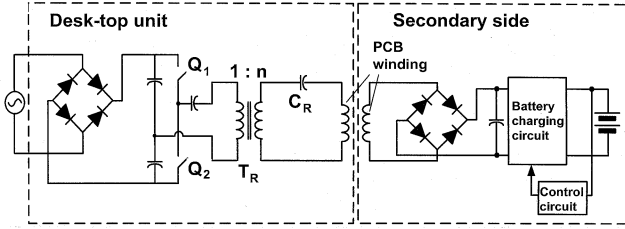
Fig. 2. Simplified circuit diagram of proposed contactless charger.

As an extension and supplement to earlier publications [4], [5], the current paper presents the practical details involved in the design and implementation of the proposed contactless battery charger. Section II addresses the general design considerations for the application circuit of the coupled PCB windings, then the circuit topology adapted to the prototype charger is presented. A series of design-oriented analyses of the proposed contactless charger are performed in Section III, along with the development of a linear circuit model for the contactless charger and its subsequent use to establish a design method for the prototype charger. Finally, Section IV demonstrates the operation and performance of the prototype charger, thereby substantiating the application potential of the contactless charging scheme using neighboring PCB windings.

II. CONTACTLESS BATTERY CHARGER

As an energy transfer device, the function of coupled PCB windings is essentially identical to that of a conventional transformer. However, due to the presence of a separation and the absence of a magnetic core between the PCB windings, coupled PCB windings exhibit unique device properties. As will be detailed in Section III, coupled PCB windings can be considered as a transformer with a large leakage inductance and small magnetizing inductance. A large leakage inductance can incur a substantial increase in the power loss, component stress, and switching noise in the application circuit [6], [7]. To resolve this problem, the application circuit can employ resonant or soft-switching converter topologies that absorb the leakage inductance as a circuit component. Conversely, a small magnetizing inductance causes a large current to circulate within the application circuit. In turn, this large circulating current induces significant conduction losses at parasitic components in the application circuit, particularly an excessive ohmic loss at the cupper traces of the PCB windings. Accordingly, certain design considerations need to be incorporated in the application circuit to restrict the circulating current to an acceptable level.

Fig. 2 shows a simplified circuit diagram of the proposed contactless battery charger. The desk-top unit consists of a line-frequency rectifier, high-frequency inverter, and the primary PCB winding. A half-bridge series resonant circuit is selected for the inverter topology as it utilizes the leakage inductance of the PCB windings as an element of the resonant tank circuit. The use of a resonant circuit also has advantages in that it minimizes the harmonic components in the circuit waveforms, thereby easing the electromagnetic interference (EMI) problem that can be incurred by the PCB windings in operation. In addition, a half-bridge series resonant circuit readily achieves a high-frequency

operation, which is essential to reduce the circulating current. A conventional step-down transformer, T_R, is inserted between the half-bridge switch network and the resonant tank circuit to further reduce the circulating current.

The secondary side of the charger includes the secondary PCB winding, a high-frequency rectifier, and battery-charging circuit. The battery charging circuit is designed using an LT1571-5 [8], which contains all the power switches, pulsewidth-modulation block, feedback control circuit, and other circuits needed to monitor and control the charging current. The battery charging circuit employs a synchronous buck converter to enhance its efficiency. In this particular application, it was possible to miniaturize the secondary side of the charger to the extent that the entire secondary part of the charger was installed inside the battery pack.

The desk-top unit operates in an open-loop condition and all the functions required to monitor and control the charging current are implemented in the battery charging circuit. Accordingly, the desk-top unit and secondary side of the charger are fully isolated in their functions, thereby eliminating the need for an additional information exchange [9] between them. The operational conditions and circuit parameters of the prototype charger are summarized in Table I. As shown in Table I, the output voltage of the high-frequency rectifier should remain within an 8 ~ 20-V range to ensure the reliable operation of the LT1571-5 used in the battery-charging circuit.

III. DESIGN-ORIENTED ANALYSIS

This section presents the modeling, analysis, and design of the proposed contactless battery charger. Based on the circuit analysis results, a design method is established that offers efficient operation for the proposed charger under all operating conditions.
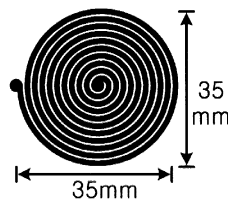
A. PCB Windings and Circuit Model

Table II shows the physical and electrical parameters of the PCB windings used in the prototype charger. The PCB windings are fabricated on a single-sided PCB with a 1-mm laminate thickness and 3-oz/ft^2 cupper layer. The dimensions and geometry of the cupper traces are empirically determined considering the operating conditions of the charger and circuit properties of the PCB windings. Since the power-handling capacity of the PCB windings is proportional to the area of the cupper traces [2], the size of the PCB windings should be designed according to the power requirements of the application system. In the current design, however, the PCB windings are oversized in an attempt to ensure the continuous operation of the battery charger even with a considerable misalignment between the PCB windings. Details on this point are presented in Section III-C. The 35-mm-diameter spiral PCB windings used in the prototype charger were in fact tested to deliver a 24-W output power at a 68% efficiency with the cupper traces 2.4 mm apart. The geometry of the cupper traces directly affects the circuit properties of the PCB windings. Many turns of thin cupper traces enhances the inductive parameters of the PCB windings, however, this design also increases the winding resistances. Therefore, the turns and width of the cupper traces were designed based on an ex-

TABLE I
OPERATIONAL CONDITIONS AND CIRCUIT PARAMETERS OF PROTOTYPE CHARGER

Desk-top unit	Secondary side
Input voltage: $85 - 270\ V_{ac}$ Switching frequency: $f_S = 950\ kHz$	Output voltage of high-frequency rectifier circuit: $8 \sim 20\ V_{dc}$ Input current of battery charging circuit: $0.1 \sim 0.35\ A_{dc}$

Circuit components:
 	
$Q_1 \sim Q_2$: IRF840
 	
$C_R : 40\ nF$
 	
$n = 0.1$
	Control IC: LT1571-5
	
	Battery:
	
	   Type: 3.3W Li-ion
	
	   Dimension: $55\,mm \times 31\,mm \times 5.5\,mm$
	
	   Voltage: $3.6 \sim 4.2\ V$
	
	   Charging current: $0.8A$ @ fast charging

TABLE II
PHYSICAL AND ELECTRICAL PARAMETERS OF PCB WINDINGS

Physical parameters of PCB windings		
Primary winding	35 mm / 35mm	Cupper trace thickness : $90\ \mu m$ Number of trace turns : 14 Separation between traces : $0.43\ mm$ Trace width : $0.82\ mm$
Secondary winding	Same as primary winding	
Electrical parameters of PCB windings with 2.4 mm separation		
$L_k = 1.46\,\mu H$, $L_m = 1.02\ \mu H$, $a = 1.57$, $R_p = R_s = 0.28\ \Omega$		

perimental tradeoff study on the performance of the PCB windings in the prototype charger. The effects of the dimension and patterns of cupper traces on the properties of neighboring PCB windings were covered in [10].

Fig. 3 shows a circuit model for the neighboring PCB windings. The circuit model is developed using the conventional method [11] that has been used to model magnetically coupled inductors. Referring to Fig. 3, the inductive parameter L_k is referred to as the leakage inductance, while L_m is called the magnetizing inductance, following the terminologies used to quantify the nonideal characteristics of conventional transformers. The circuit parameters shown in Fig. 3 can be either analytically calculated [12] or experimentally measured [2]. The model parameters measured from the PCB windings separated from each other by 2.4 mm (the laminate thickness of the two PCBs plus a 0.4-mm distance between the PCBs) are listed in Table II. Interestingly, the leakage inductance, $L_k = 1.46\ \mu H$, is larger
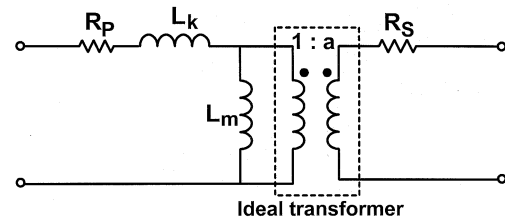

Fig. 3.   Circuit model for neighboring PCB windings.

than the magnetizing inductance, $L_m = 1.06\ \mu H$. These unique characteristics are attributed to the existence of a separation and the absence of a magnetic core between the PCB windings. The winding resistances, $R_p = R_s = 0.28\ \Omega$, are also important circuit parameters as the ohmic loss in the PCB windings can be a major source of power losses.
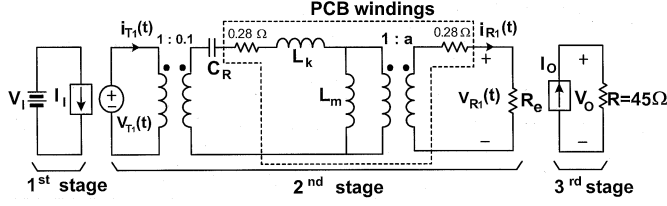
Fig. 4.   Linear circuit model of proposed battery charger.

TABLE III
CIRCUIT VARIABLES AND PARAMETERS FOR CIRCUIT MODEL OF
CONTACTLESS CHARGER

	Expressions
First stage	$V_I = \dfrac{\|v_S\|}{2}, \ I_I = \dfrac{2\,I_{T1}}{\pi} cos\,\varphi_T$ $\|v_S\|$: Amplitude of line voltage
Second stage	$v_{T_1}(t) = \dfrac{4V_I}{\pi} sin\,\omega_s t$ $i_{T_1}(t) = I_{T_1}\, sin(\omega_s t - \varphi_T)$ $v_{R_1}(t) = V_{R_1}\, sin(\omega_s t - \varphi_R)$ $i_{R_1}(t) = I_{R_1}\, sin(\omega_s t - \varphi_R)$ $R_e = \dfrac{8}{\pi^2}R$
Third stage	$I_O = \dfrac{2}{\pi}I_{R1} \ , \quad R = \dfrac{V_O}{I_O}$

B. Circuit Model for Battery Charger

Fig. 4 shows a linear circuit model for the proposed contactless charger. The model is created by adapting the circuit model of the PCB windings to the well-known modeling technique [13], [14] for resonant converters. The model consists of three stages. The first stage is a dc model that represents the dc characteristics of the line-frequency rectifier and half-bridge switch network. The second stage is an ac model that describes the relationships between the fundamental components of the circuit variables associated with the PCB windings, based on the assumption that the higher order harmonics of the circuit variables are well suppressed by the resonant tank circuit thus only the fundamental components are present in the circuit. The third stage models the functional behavior of the battery charging circuit. The third stage terminates with an equivalent load resistor, given by $R = V_O/I_O$ with V_O representing the output voltage of the high-frequency rectifier and I_O denoting the input current to the battery charging circuit. The typical operating point of the battery charging circuit is located at $V_O = 13$ V and $I_O = 0.29$ A, thereby resulting in $R = 45\ \Omega$. The expressions for the circuit variables and parameters appearing in Fig. 4 are given in Table III.
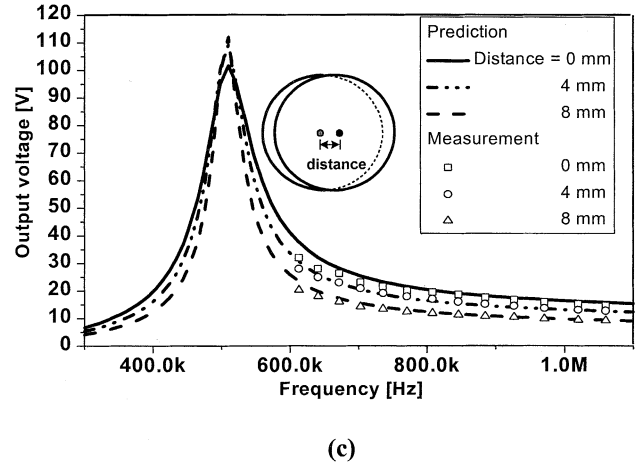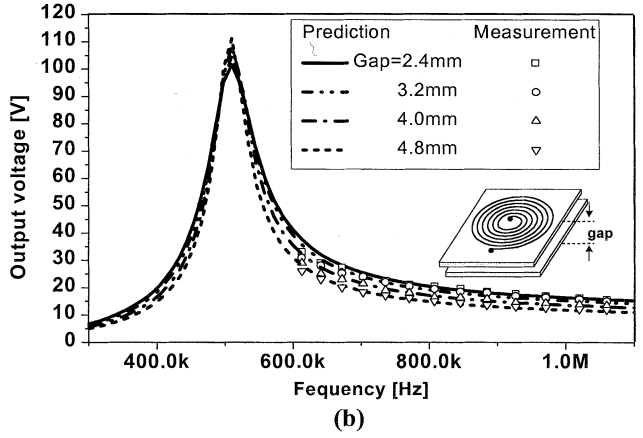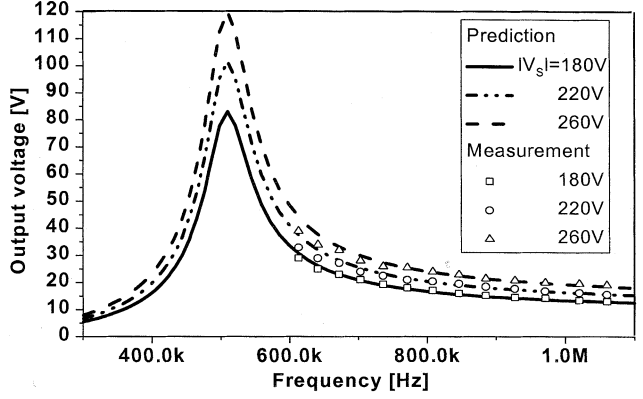

(a)

(b)

(c)

Fig. 5.   Output voltage of high-frequency rectifier. (a) Output voltage with different line voltages. (b) Output voltage with different gaps. (c) Output voltage with different distances.

C. Voltage Transfer Gain of Contactless Charger

In this section, the voltage transfer gain of the contactless charger is analyzed using its linear circuit model. The results of the analysis are then used to determine the switching frequency of the prototype charger. From Fig. 4, the voltage transfer gain from the line voltage to the output voltage of the high-frequency rectifier can be recognized as

$$M = \frac{V_O}{|v_S|} = \left(\frac{V_I}{|v_S|}\right)\left(\frac{V_{T_1}}{V_I}\right)\left(\frac{V_{R1}}{V_{T1}}\right)\left(\frac{I_{R_1}}{V_{R1}}\right)\left(\frac{I_O}{I_{R1}}\right)\left(\frac{V_O}{I_O}\right).$$
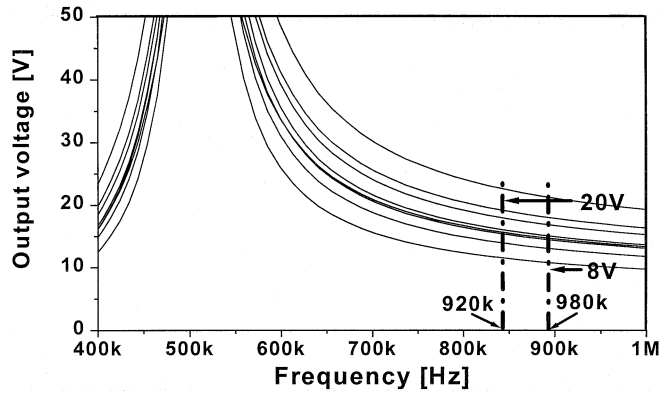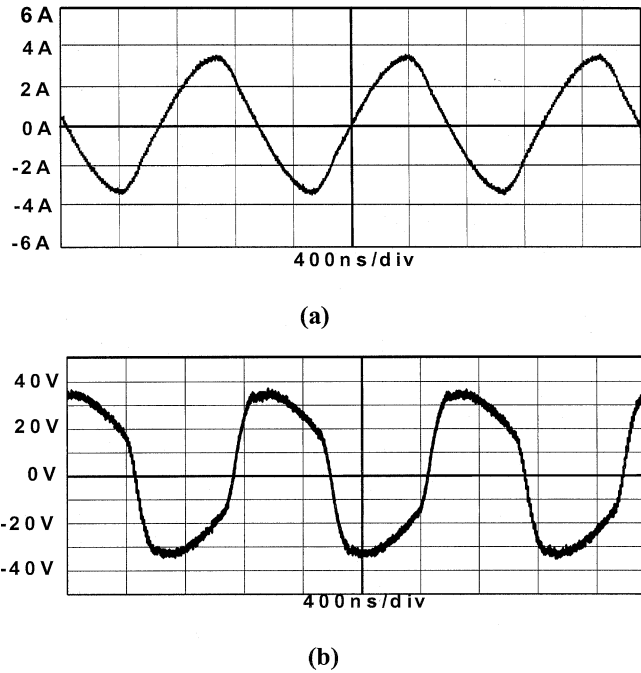
(1)

Fig. 6.   Collection of output voltage curves.

(a)

(b)

Fig. 7.   Current and voltage waveform of primary PCB winding. (a) Current: 2 A/div, 400 ns/div. (b) Voltage: 10 V/div, 400 ns /div.
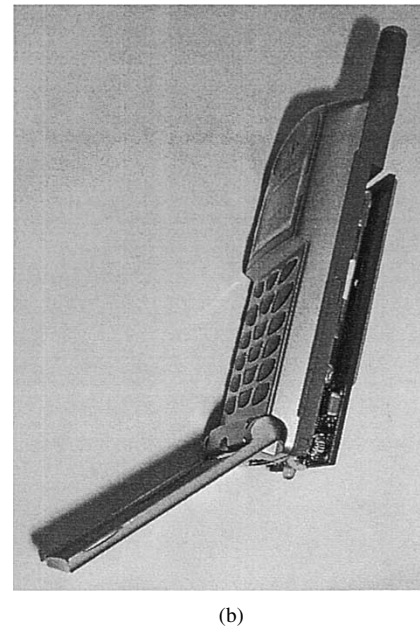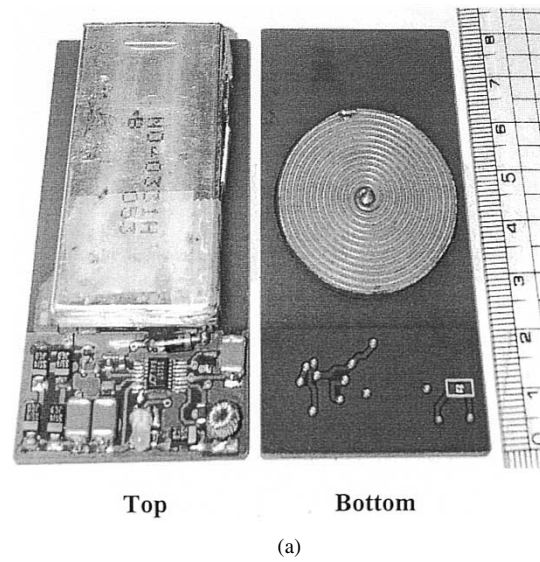

Top   **Bottom**

(a)

(b)

Fig. 8.   Secondary side of prototype contactless charger developed for cellular phones. (a) Secondary side of charger. (b) Cellular phone equipped with secondary side of charger.

Using the expressions given in Table III, the voltage transfer gain can be evaluated as

$$M = 0.5 \frac{4}{\pi} H(s) \frac{\pi^2}{8R} \frac{2}{\pi} R = 0.5\, H(s) \qquad (2)$$

where $H(s)$ is the input-to-output transfer function of the second-stage ac model. By evaluating $|H(s)|_{s=j\omega_s}$, the magnitude of the voltage transfer gain can be expressed as a function of the switching frequency ω_s

$$|M| = \frac{0.05}{\left| \left(\frac{L_k+L_m}{aL_m} - \frac{1}{\omega_s^2 aC_R L_m} \right) + j \left(\frac{a\omega_s L_k}{R_e} - \frac{a}{\omega_s C_R R_e} \right) \right|}. \qquad (3)$$

Equation (3) can now be used to predict the output voltage of the high-frequency rectifier under various operating conditions. Fig. 5(a) shows the output voltage curves evaluated when the line voltage varies from $|V_s| = 180$ V to $|V_s| = 260$ V while

the separation between the PCB windings is fixed at 2.4 mm. Each theoretical curve is compared with experimental data measured using the prototype charger in which the output terminals of the high-frequency rectifier are connected to a 45-Ω resistor. Since theoretical transfer curves are only valid for frequencies above the resonance frequency of the LC tank [13], the curves are experimentally verified at frequencies higher than 600 kHz. The experimental data exhibit a good correlation with the analytical predictions, thereby validating the modeling and analysis method.

Fig. 5(b) shows the output voltage curves evaluated when the separation between the PCB windings is varied between 2.4 mm < gap < 4.8 mm [the definition for "gap" is shown in Fig. 5(b)], while the line voltage is fixed at $|V_s| = 220$ V. Each theoretical curve is obtained by evaluating (3) using the circuit parameters measured with a different separation between the
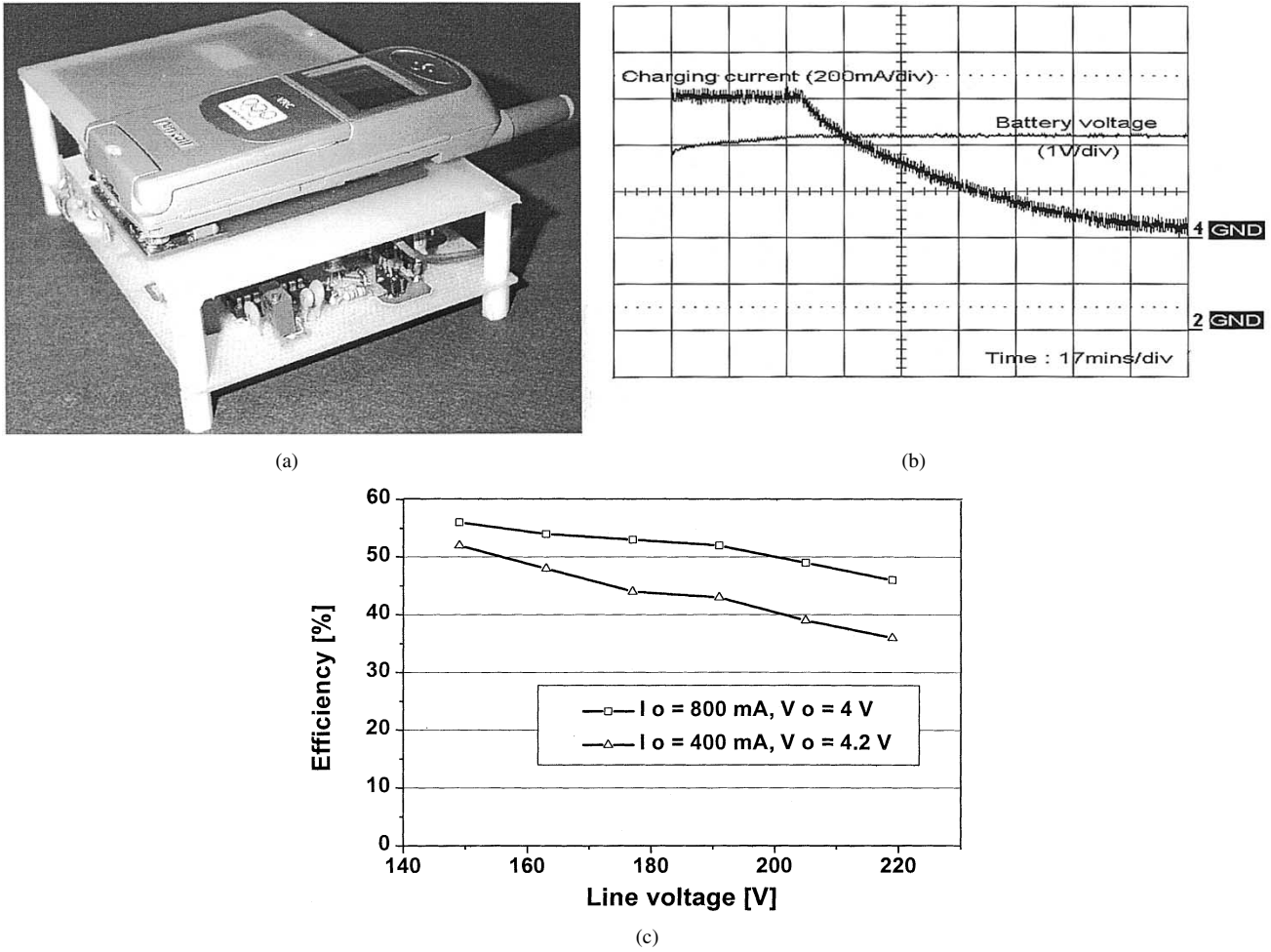
(a)

(b)

(c)

Fig. 9.   Prototype charger and its performance. (a) Prototype charger in operation. (b) Charging profile. (c) Efficiency.

PCB windings. Fig. 5(c) shows the analysis results of the circuit in which the separation is fixed at 2.4 mm and the line voltage set at $|V_s| = 220$ V, yet the cupper traces are off center due to the misalignment of the PCB windings. Fig. 5(c) shows the output voltage curves when the lateral distance between the centers of the cupper traces is varied between 0 mm < distance < 8 mm; the definition for "distance" is illustrated in Fig. 5(c).

As emphasized in Section II, the output voltage of the high-frequency rectifier should be limited within an 8~20-V range for a stable operation of the control IC inside the battery charging circuit. Fig. 6 shows a collection of all the output voltage curves analyzed in Fig. 5(a)–(c). As illustrated in Fig. 6, when the switching frequency is set at a frequency within a 920~980-kHz range, the output voltage of the high-frequency rectifier never exceeds the 8~20-V boundary. Based on this analysis, the switching frequency of the inverter is chosen to be $f_s = 950$ kHz. This design strategy provides a stable operation for the charger under all operating conditions without requiring an additional feedback path [9] between the desk-top unit and the secondary side of the charger. Since the switching frequency is selected well above the resonant frequency of the tank circuit, this design also provides a zero-voltage switching condition for the switch network [14] and offers high impedance characteristics for the resonant thank circuit [15], thereby reducing the circulating current in the circuit.

IV. PERFORMANCE OF PROTOTYPE CHARGER

This section describes the operation and performance of the prototype battery charger under various operating conditions. Fig. 7 shows the current and voltage waveform of the primary PCB winding measured when $|V_s| = 220$ V, $R = 45\ \Omega$, and with a 2.4-mm separation between the PCB windings. The current passing through the primary winding [Fig. 7(a)] is almost a sinusoidal wave. The voltage across the primary winding [Fig. 7(b)] is also smoothly filtered by the inductances of the PCB windings. As such, these continuous and smooth waveforms alleviate the possible EMI problems associated with the PCB windings in operation.

Fig. 8(a) shows the secondary side of the prototype charger fabricated on a double-sided PCB. A 3.3-W lithium-ion battery along with the battery-charging circuit is placed on the front side, while the secondary PCB winding is printed on the opposite side. Fig. 8(b) shows a cellular phone equipped with the secondary side of the prototype charger. As shown in Fig. 8(b), the secondary side of the charger is naturally suited for a low-profile design and therefore can readily be encapsulated within a standard battery pack without causing any major heat management problems.

Fig. 9(a) shows the proposed contactless charging system in operation. The prototype charger was not found to have any

adverse effect on the performance of the cellular phone. No perceptible consequences of EMI were observed during the field tests, however, a newly proposed shielding technique [3] using a ferrite polymer composite sheet could be adapted for PCB windings to suppress the leakage flux to a negligible level. Fig. 9(b) shows the charging characteristics of the prototype charger that goes through a transition from constant-current charging to constant-voltage charging. The charger exhibited a precisely controlled charging profile. Fig. 9(c) shows the efficiency of the proposed charger measured under two different conditions: constant-current charging [upper curve in Fig. 9(c)] and constant-voltage charging [lower curve in Fig. 9(c)]. A maximum efficiency of 57% was measured during the constant-current charging mode. In these measurements, a dc voltage source was used as a substitute for the rectified line voltage.

V. CONCLUSION

This paper has demonstrated a practical contactless charger, applicable to most low-profile hand-held electronics as well as cellular phones, which is implemented using two neighboring PCB windings as the energy transfer device. The efficient operation of the prototype contactless charger was also confirmed, even with a considerable separation and misalignment between the PCB windings, when the PCB windings, energy transfer circuit, and battery charging circuit were systematically and harmoniously designed. The main features of the prototype charger presented in this paper are summarized below.

- The secondary side of the charger is fabricated in a low-profile fashion, thereby allowing the entire secondary part of the charger to be encapsulated within a standard battery pack.
- The power loss in the prototype charger is kept at a low level to avoid any major thermal problems. A series resonant circuit is used for the energy transfer circuit and a synchronous buck converter is adapted for the battery charging circuit to minimize the power losses.
- The prototype charger does not necessitate any information feedback between the primary and secondary side of the charger. This significantly simplifies the design and operation of the charger, when compared to other contactless chargers that require a feedback path to control the battery charging current.
- The prototype charger does not cause any perceptible EMI problems, primarily due to the use of a series resonant circuit that generates continuous and smooth waveforms with negligible high-frequency harmonic components.

ACKNOWLEDGMENT

REFERENCES

[1] S. Y. R. Hui, S. C. Tang, and H. Chung, "Coreless printed-circuit board transformers for signal and energy transfer," *Electron. Lett.*, vol. 34, no. 11, pp. 1052–1054, 1998.

[2] ——, "Optimal operation of coreless PCB transformer-isolated gate drive circuit with wide switching frequency range," *IEEE Trans. Power Electron.*, vol. 14, pp. 506–514, May 1999.

[3] S. C. Tang, S. Y. R. Hui, and H. Chung, "A low-profile power converter using printed-circuit board (PCB) power transformer with ferrite polymer composite," *IEEE Trans. Power Electron.*, vol. 16, pp. 493–498, July 2001.

[4] B. Choi and J. Nho, "Contactless energy transfer using planer printed circuit board windings," *Electron. Lett.*, vol. 37, no. 16, pp. 1007–1009, 2001.

[5] B. Choi, H. Cha, J. Nho, and S. Park, "A new contactless battery charger for portable telecommunication/computing electronics," in *Proc. IEEE ICCE'01*, June 2001, pp. 58–59.

[6] D. G. Pedder, A. D. Brown, and J. A. Skinner, "A contactless electrical energy transmission system," *IEEE Trans. Ind. Electron.*, vol. 46, pp. 23–30, Feb. 1999.

[7] Y. Jang and M. M. Jovanivic, "A contactless electrical energy transmission system for portable-telephone battery chargers," in *Proc. INTELEC'00*, 2000, pp. 726–732.

[8] "LT1572 data sheet," Linear Technology Co., Milpitas, CA, 2000.

[9] C. Kim, D. Seo, J. You, J. Park, and B. H. Cho, "Design of a contactless charger for cellular phone," *IEEE Trans. Ind. Electron.*, vol. 48, pp. 1238–1247, Dec. 2001.

[10] C. Fernandez, O. Garcia, R. Prieto, J. A. Cobos, S. Gabriels, and G. Van Der Borght, "Design issues of a coreless transformer for a contactless application," in *Proc. APEC'02*, 2002, pp. 339–345.

[11] J. W. Nilsson and S. A. Riedel, *Electronic Circuits*, 6th ed. Upper Saddle River, NJ: Prentice-Hall, 2001, pp. 993–1001.

[12] W. G. Hurley and M. C. Duffy, "Calculation of self and mutual inductances in planar magnetic structures," *IEEE Trans. Magn.*, vol. 31, pp. 2416–2422, July 1995.

[13] R. L. Steigerwald, "A comparison of half-bridge resonant converter topologies," *IEEE Trans. Power Electron*, vol. 3, pp. 174–182, Apr. 1988.

[14] R. W. Erickson and D. Maksimovic, *Fundamentals of Power Electronics*, 2nd ed. Norwell, MA: Kluwer, 2001, ch. 19.

[15] M. K. Kazimierczuk and T. Nandakumar, "Class D voltage switching inverter with tapped resonant inductor," *Proc. Inst. Elect. Eng.*, pt. B, vol. 140, no. 3, pp. 177–185, May 1993.

Byungcho Choi (S'90–M'91) received the B.S. degree in electronics from Hanyang University, Seoul, Korea, in 1980, and the M.S. and Ph.D. degrees in electrical engineering from Virginia Polytechnic Institute and State University, Blacksburg, in 1988 and 1992, respectively.

From 1992 to 1993, he was a Research Scientist with the Bradley Department of Electrical Engineering, Virginia Polytechnic Institute and State University. From 1994 to 1995, he served as a Team Leader of the Power Electronics Systems Team at Samsung Electronics Company. In 1996, he joined the School of Electronic and Electrical Engineering, Kyungpook National University, Taegu, Korea, where he is presently an Associate Professor. His research interests include modeling and design optimization of high-frequency power converters for portable electronics, computer power systems, and distributed power systems.
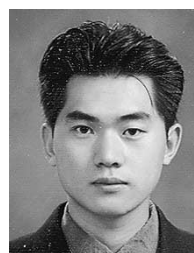
Jaehyun Nho received the B.S. degree in electronic engineering from Taegu University, Taegu, Korea, in 1994, and the M.S. degree in electrical engineering from Kyungpook National University, Taegu, Korea, in 2002.

He is presently with LG Electronics, Gumi-city, Korea, where he is involved with the development of power conditioning and driving circuits for ac plasma display panel (PDP) application systems. His research interests include modeling, analysis, and design of low-profile power converters and driving circuits for large-diagonal PDP application systems.

Honnyong Cha received the B.S. and M.S. degrees in electrical engineering in 1999 and 2001, respectively, from Kyungpook National University, Taegu, Korea, where he is currently working toward the Ph.D. degree.

From 2001 to 2003, he was a Research Engineer with Power System Technology Company, Ansan-city, Korea, where he was involved with the development of power electronics application systems. His research interests include modeling, analysis, and design of resonant power conversion circuits.

Seungwon Choi (M'91) received the B.S. degree in electronics engineering from Hanyang University, Seoul, Korea, in 1980, the M.S. degree in electronics engineering from Seoul National University, Seoul, Korea, in 1982, and the M.S. degree in computer engineering and the Ph.D. degree in electrical engineering from Syracuse University, Syracuse, NY, in 1985 and 1988, respectively.

From 1988 to 1989, he was with the Department of Electrical and Computer Engineering, Syracuse University, as an Assistant Professor. In 1992, he joined Hanyang University as an Assistant Professor. He is currently a Professor in the School of Electrical and Computer Engineering. His research interests include digital communications and adaptive signal processing with a recent focus on the real-time implementation of the smart antenna systems for 3G mobile communication systems.

Taeyoung Ahn (M'88) received the B.S. and M.S. degrees from Hanyang University, Seoul, Korea, in 1984 and 1990, respectively, and the Ph.D. degree from Kyushu University, Kyushu, Japan, in 1994, all in electronics engineering.

In 1997, he joined the School of Computer and Communication Engineering, Chongju University, Cheongju, Korea, where he is currently an Assistant Professor. His main research interests include modeling, design, and performance evaluation of board-mount switching power converters for telecommunication applications.